



# Lawrence Berkeley Laboratory

UNIVERSITY OF CALIFORNIA

## Materials & Molecular Research Division

Submitted to the Journal of the Electrochemical Society

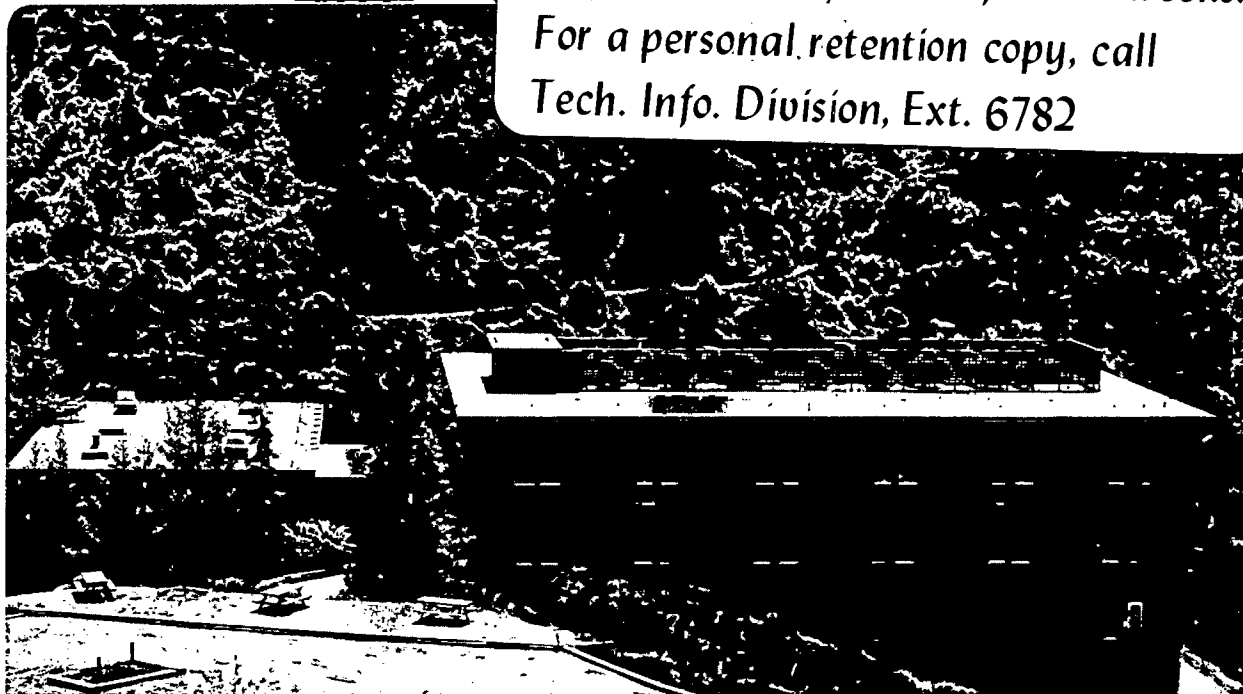
INTERFEROMETRIC STUDY OF COMBINED FORCED  
AND NATURAL CONVECTION

F.R. McLarnon, R.H. Muller, and C.W. Tobias

August 1981

RECEIVED  
PHYSICS  
LABORATORY  
OCT 2 1981  
DOCUMENTS SEC

**TWO-WEEK LOAN COPY**  
*This is a Library Circulating Copy  
which may be borrowed for two weeks.  
For a personal retention copy, call  
Tech. Info. Division, Ext. 6782*



LBL-13032  
c2

## DISCLAIMER

This document was prepared as an account of work sponsored by the United States Government. While this document is believed to contain correct information, neither the United States Government nor any agency thereof, nor the Regents of the University of California, nor any of their employees, makes any warranty, express or implied, or assumes any legal responsibility for the accuracy, completeness, or usefulness of any information, apparatus, product, or process disclosed, or represents that its use would not infringe privately owned rights. Reference herein to any specific commercial product, process, or service by its trade name, trademark, manufacturer, or otherwise, does not necessarily constitute or imply its endorsement, recommendation, or favoring by the United States Government or any agency thereof, or the Regents of the University of California. The views and opinions of authors expressed herein do not necessarily state or reflect those of the United States Government or any agency thereof or the Regents of the University of California.

INTERFEROMETRIC STUDY OF COMBINED  
FORCED AND NATURAL CONVECTION

by

F. R. McLarnon,\* R. H. Muller and C. W. Tobias

Materials and Molecular Research Division  
Lawrence Berkeley Laboratory  
and Department of Chemical Engineering  
University of California  
Berkeley, CA 94720

\* Energy and Environment Division  
Lawrence Berkeley Laboratory  
Berkeley, CA 94720

Key Descriptors: Interferometry; Mass Transfer; Forced  
Convection; Natural Convection.

CONTENTS

	<u>PAGE</u>
I. Abstract	1
II. Introduction	2-5
III. Experimental	5-8
IV. Results and Discussion	9-14
V. Conclusion	15

ABSTRACT

When a metal is electrodeposited in laminar flow onto a planar cathode facing upward in a channel, mass transfer rates are enhanced downstream beginning at some distance from the leading edge, because of the contribution of free convection to the fluid motion. The position and extent of this secondary flow has been clearly demonstrated by double beam interferometry, employed for the measurement of concentration profiles in the cathodic boundary layer. A narrow range of critical Rayleigh numbers,  $1270 \pm 200$ , has been associated with the onset of natural convection. This result provides a convenient basis for the prediction of the transition from forced convection control to combined forced and natural convection control of the mass transfer process.

## INTRODUCTION

The rates of many electrochemical processes, such as electrodeposition and electro-organic syntheses, are limited by slow mass transfer. An understanding of transport phenomena occurring near electrode surfaces is therefore essential to the economic design of electrochemical cells. A specific example of such a process is electroplating on vertical plates in unstirred electrolytes, which has long been known (1-3) to be rate-limited by natural convection mass transfer. Many recent studies have been conducted with the ultimate aim of understanding the complex relationship between the velocity profile in the hydrodynamic boundary layer (4-6), the concentration profile in the mass transfer boundary layer (7-10), and the distribution of current density along the vertical electrode surface (11-13). Such studies have contributed to the design of electroplating cells.

The parallel plate geometry is commonly employed in industrial electrochemical processes (14). Many novel cell designs aimed at enhancing mass transfer rates have been invented in recent years, e.g. using magnetic fields (15), wiped plates (16), very high flow rates (17), ultrasonic waves (18), and controlled abrasion of the plate (19). One method of improving the mass transport conditions in a parallel plate (rectangular duct) electrolysis cell is to orient the cell so that the less dense electrolyte solution is produced below electrolyte of higher density, e.g. by employing an upward facing cathode in electrodeposition. The resulting buoyant forces

can lead to natural convection, which increases the transport rate above that due to forced convection. This combined mode of mass transfer can be expected to be important in electrolytic processes which employ low electrolyte flow and large density gradients.

Tobias and Hickman (20) employed the limiting current technique and a sectioned cathode to study ionic mass transport by combined free and forced convection using a model reaction: the electrodeposition of Cu from aqueous solutions of  $\text{CuSO}_4$ ,  $\text{H}_2\text{SO}_4$  and glycerol. The resulting distribution of limiting current density along the length of the sectioned electrode exhibited a strong dependence upon cell orientation (cathode facing up vs. cathode facing down) and the concentration, velocity and viscosity of the electrolyte. The mass transfer enhancement by natural convection effects at the upward-facing sectioned cathode was recognized as a limiting current density up to three times larger than the corresponding value at a downward-facing cathode, where the mass transfer process is controlled by forced convection alone. Onset of natural convection effects occurred at a considerable distance (up to 20 cm) downstream from the electrode leading edge and was linked to a streaked deposit (parallel grooves in the flow direction) on the plate. This phenomenon was explained in terms of secondary convective flows (roll cells.) It was postulated that these cells form when the local

mass transfer boundary layer thickness grows thick enough that the critical Rayleigh number, which determines the hydrodynamic stability of the system, is exceeded. The local mass transfer boundary layer thickness  $\delta$  was suggested as the characteristic dimension to employ in the definition of the Rayleigh number. Tobias and Hickman estimated the diameter of these roll cells to be of the order of 0.5 mm.

In the present work the interferometric method (21, 22) is applied to the study of combined forced and natural convection in a rectangular-duct flow channel. In this technique, variations in the phase of transmitted light normal to the direction of light propagation are measured. The corresponding variations in local refractive index (linearly related to electrolyte concentration over the concentration range employed in this work) are subsequently derived from the observation. This method thereby provides direct, continuous visualization of the local concentration boundary layer at any level of current density on continuous, (unsectioned) electrodes. Even if the experimental interferograms are not amenable to complete quantitative interpretation, which will be seen to be the case when substantial natural convection effects are present, significant qualitative information can be gleaned from the data. The immediate goals of this work are to (a) conduct an optical search for the onset of natural convection effects and determine a predictive basis for its occurrence, (b) examine the structure (e.g. evidence of roll cells) of the mass transfer boundary layer when natural convection effects are present, and (c) attempt to determine an appropriate characteristic boundary layer dimension to employ in the definition of the Rayleigh number.

The interferometric method has been employed by many investigators (7, 9, 10, 23-33) to measure the concentration profiles in electrochemical mass transfer boundary layers. Even though it has long been recognized (21, 22, 33-43) that light deflection (refraction, Schlieren effect) within a refractive-index field can seriously distort the resulting experimental interferograms, only a few recent studies have taken steps to account for this phenomenon (6, 9, 10, 31-33, 37-40).

## EXPERIMENTAL

(1) Flow Channel. Mass transfer experiments were carried out in a 3 m long rectangular duct flow channel (23, 44, 45), the heart of which is depicted in Figure 1. Gravity feed from a storage tank provides a steady flow of electrolyte. The duct is  $w = 1.00$  cm wide and  $h = 2.54$  cm high. The  $L = 100$  cm long electrodes fully occupy the space between the two parallel optically flat glass sidewalls downstream of a 200 cm long (140 hydraulic diameters) entry region. The physical dimensions of this electrochemical cell result in a uniform current density distribution over 99% of the electrode area (32), provided that the limiting current density is not approached at any location along the electrode surfaces.

(2) Electrolyte and Electrode Preparation. The 99.999% pure copper electrodes were designed with two goals in mind: (a) the horizontal electrode working surfaces should be flat and smooth, and (b) the test beam should traverse the cell parallel to the working surface. These requirements were met by first polishing a vertical side of each electrode flat and optically smooth. Then, a right angle-polishing jig was used to prepare the electrode working surfaces perpendicular to the reflecting sides. The cell would then be aligned so that the test beam was parallel (to within  $0.1^\circ$ ) to the electrode working surface by reflecting the beam from the side under exactly normal incidence (the reflected beam retraced its path back to its source). The working surface profile was flat to within  $1 \mu\text{m}$  over 80% of its width. However, the edges were slightly rounded (to about  $10 \mu\text{m}$ ) below the level of the center of the surface (23, 46).

The aqueous  $\text{CuSO}_4$  electrolyte was prepared by dissolving reagent grade  $\text{CuSO}_4 \cdot 5\text{H}_2\text{O}$  crystals into twice-distilled water in a 25-gal polyethylene container. The dependence of electrolyte refractive index on  $\text{CuSO}_4$  concentration was determined with an Abbé critical angle refractometer. Sample concentrations were determined by gravimetric analysis. A least-squares analysis provided the following linear correlation for the refractive index at  $\lambda = 632.8 \text{ nm}$  (He-Ne laser),  $0 \leq C \leq 0.1\text{M CuSO}_4$

$$n = 1.3311 + 0.0290 \cdot C$$

All electrolysis experiments employed 0.1 M  $\text{CuSO}_4$  electrolyte.

(3) Interferometer. A cross section of the duct and dual emission laser interferometer is shown in Fig. 2. A He-Ne laser was modified to emit light from each end, and the interferometer was mounted on a lathe bed to permit travel of the instrument along the length of the electrodes (23, 44, 45). The plane of focus (optically conjugate to the film plan of the camera) was located at the inside of the glass sidewall farthest from the camera,  $x = 0$  (Fig. 1). This is the recommended plane of focus for the observation of cathodic boundary layers in which the refractive index decreases toward the electrode surface (38).

(4) Electrochemical Experiments. Previous studies in this laboratory have focused on the transient, pure diffusion, constant-current electrodeposition of Cu from a stagnant layer of 0.1 M  $\text{CuSO}_4$  onto a downward-facing cathode (31),

and the transient and steady-state constant-current electrodeposition of Cu in laminar forced convection onto a downward-facing cathode (32). The present work examines the steady-state constant-current electrodeposition of Cu onto an upward-facing cathode for three different laminar flow rates  $Re = 500, 1000$  and  $1500$  ( $v_{avg} = 3.5, 7.0$  and  $10.5$  cm/s) at several current densities and at various distances downstream from the leading edge.

## RESULTS AND DISCUSSION

The time behavior of the mass transfer boundary layer was observed with a 16 mm movie camera at 10-30 frames/sec. Typical experimental interferograms are displayed on Fig. 3. This sequence of photographs shows the different transient behavior of the mass transfer boundary layer at downward-facing and upward-facing cathodes. The fringes are straight prior to the beginning of electrodeposition at  $t=0$ , indicating a uniform refractive-index field and a uniform concentration throughout the electrolyte (the slight displacement seen near the cathode is caused by light reflection (46) from the edge of the electrode surface).

Curved fringe patterns at  $t=10$ , 20 and 30 s represent regions of smaller electrolyte refractive index ( $\text{CuSO}_4$  concentration) near the electrode surface. The shape of the fringe pattern corresponds roughly to the  $\text{CuSO}_4$  concentration profile. Conversion of the interferograms into accurate concentration profiles requires optical analysis, details of which have been given elsewhere (40, 38, 23).

After 10 s of electrodeposition, the interference fringe patterns at upward-facing and downward-facing cathodes are similar. However, after ca 20 s of electrodeposition, a "kink" is clearly visible in the fringe pattern at the upward-facing cathode. Qualitative and semi-quantitative interpretation of the "kinked" interferograms by motion picture analysis has led to the following general observations:

1. The kinks were found to appear at well-defined locations  $z_c$  downstream from the electrode leading edge. This location was found to depend upon electrolyte flow rate and current density and is indicative of the onset of natural convection.
2. The kinks oscillated toward and away from the electrode surface at 0.01-1 Hz. For all experiments, the mean distance from the electrode surface to the kink (e.g. the minimum that appears at 0.5 mm from the electrode surface in Fig. 3,  $t=30$  s, upward-facing cathode) was 0.5 mm, and the amplitude of oscillation was 0.3 mm. It is suggested that the  $0.5 \text{ mm} \pm 0.3 \text{ mm}$  separation between the kink and the electrode surface corresponds to the average dimension of the secondary hydrodynamic flow driven by bouyant forces. This dimension corresponds to the roll cell size 0.5 mm postulated by Tobias and Hickman (20) for similar conditions of combined forced and natural convection.
3. The kinks were remarkably uniform, extending up to 10 cm in the flow direction while remaining at a constant distance from the electrode surface. This corroborates Tobias and Hickman's observations that streaked deposits (coincident with increased mass transfer rates and roll cells) can extend for many centimeters in the flow direction.

4. The effective mass transfer boundary layer thickness indicated by interferograms that display kinks is substantially less than the corresponding thickness at the downward facing cathode. An approximate measure of this reduction is the effective (Nernst) boundary layer thickness, which is obtained by extrapolating the nearly linear fringe slope seen at the electrolyte/electrode interface (see Fig. 7, below). The reduced Nernst layer thickness corresponds to increased values of limiting current density, as observed by Tobias and Hickman. The present studies were performed at current densities well below limiting values, which leads to a very uniform current density distribution (32), whereas Tobias and Hickman's data were obtained at the local value of the limiting current density, which leads to a highly non-uniform current density distribution.

In contrast to prior success in the reduction of experimental interferograms to accurate concentration profiles and mass transfer rates in pure diffusion (31) and laminar forced convection (32) regimes, an exact analysis of the kinked fringes was not possible. This result could be expected, because the interferometric measurements result in a two-dimensional representation of a three-dimensional concentration field. Refractive-index information is averaged along the optical path of the test beam with the stirring action of the roll cells leading to substantial variations along the optical path.

It was possible, however, to analyze interferograms of the mass transfer boundary layer at locations upstream ( $z < z_c$ ) of the region  $z_c < z < L$  where kinks appeared in the interferograms. From this analysis, precise information about the boundary layer structure (boundary layer thickness,  $\text{CuSO}_4$  surface concentration, current density) could be obtained. These data are particularly useful for subsequent computation of local Rayleigh Numbers (see below).

Figures 4 and 5 provide comparisons between local Nernst boundary layer thickness derived from experimental interferograms, represented by the data points, and the local Nernst thickness predicted for laminar forced convection conditions by the well-known Norris-Streid correlation (47), represented by the solid lines. The open circles shown in Fig. 4 are experimental local boundary layer thicknesses at a downward-facing cathode, and they show agreement with the Norris-Streid correlation, as expected (32).

The filled symbols shown in Figures 4 and 5 are experimental boundary layer thicknesses at upward facing cathodes for two different laminar flow rates, and the dashed curves are drawn to show the trend of the data for different current densities. These data indicate two separate regimes of mass transfer control: (a) near to the cathode leading edge, the data follow the Norris-Streid correlation, confirming that the electrodeposition process is dominated by laminar forced convection in this region, and (b) far downstream, the boundary layer thickness is relatively uniform ( $\delta_N = 0.14 \pm 0.03$  mm for  $\text{Re} = 500$ ,  $\delta_N = 0.10 \text{mm} \pm 0.02$  mm for  $\text{Re} = 1500$ ), and the mass transfer process is under combined forced and natural convection control. The location  $z = z_c$  (indicated by the maxima in the dashed

curves shown in Figures 4 and 5) separates the two regions of mass transfer control. At a fixed flow,  $z_c$  moves further upstream at higher levels of applied current density.

Smoothed limiting current data obtained on a segmented electrode by Tobias and Hickman (20) are plotted in Figure 6. The transition between forced convection and combined forced and natural convection control corresponds to the minima exhibited by the dashed curves in Figure 6. Tobias and Hickman's data for 0.11  $\text{CuSO}_4$  and  $\text{Re} = 1400$  show a transition location  $z_c = 7$  cm and a local limiting current density of  $10 \text{ mA/cm}^2$ , which compares favorably with the location  $z_c = 8$  cm shown in Figure 5 for 0.10 M  $\text{CuSO}_4$ ,  $\text{Re} = 1500$  and  $i = 10 \text{ mA/cm}^2$ .

An appropriate measure of the driving force for natural convection is the Rayleigh Number

$$\text{Ra} = \text{Gr Sc} = \frac{g \cdot \delta_c^3 \cdot \Delta \rho}{\nu^2 \rho} \frac{\nu}{D} = \frac{g \cdot \delta_c^3 \cdot \alpha \cdot \Delta C}{\mu D}, \quad (\text{Eq. 1})$$

where  $\delta_c$  is a characteristic distance over which the density difference  $\Delta \rho$  is manifest,  $\Delta C$  is the local concentration difference and  $\alpha$  is a proportionally constant relating density differences to concentration changes. The other terms have their conventional meanings (see List of Symbols). The proportionally constant  $\alpha$  has been derived from literature data (48) over the range  $0 < C < 0.1 \text{ M CuSO}_4$ :

$$\alpha = 0.155 \text{ gm cm}^{-3} (\text{M CuSO}_4)^{-1} \quad (\text{Eq. 2})$$

Rayleigh Numbers were computed from (a) the electrolyte physical properties (48), (b) concentration differences  $\Delta C$  measured at the transition locations  $z_c$ , and the (c) characteristic boundary layer thickness  $\delta_c$  measured at (or just upstream of) the transition location  $z_c$ . Note that the concentration profiles are derived from interferograms without kinked contours.

The characteristic boundary-layer thickness  $\delta_c$  was chosen as the region which contains 90% of the concentration difference measured from the interface toward the bulk solution (the 90% boundary layer thickness). The edge of this layer is indicated by the open circle in Figure 7. The concentration contour shown in Figure 7 is a Pohlhausen-type profile,

$$\theta = 2Y - 2Y^3 + Y^4 \quad (\text{Eq. 3})$$

where  $\theta$  is a dimensionless concentration and  $Y$  is a reduced distance from the electrode surface. This form was found to accurately describe the concentration contour in laminar forced convection mass transfer boundary layers (32) and is an excellent approximation to the solution (32, 49, 23) of the equation of convective diffusion for constant-current, laminar forced convection conditions. The 90% boundary layer edge can be identified with the linear concentration profile designated by a series of short and long dashes in Figure 7. This linear profile is equivalent to the Pohlhausen profile in the sense that the two cross-hatched regions are of equal area.

The Rayleigh Numbers computed from the experimental interferograms obtained at the various transition locations  $z_c$  are listed in Table 1. All but one of the Rayleigh Numbers fall into the range  $Ra = 1270 \pm 200$ , which indicates a well-defined criterion for the observed onset of natural convection effects. Previous computations (50) of critical Rayleigh Numbers in horizontal, parallel-plate electrochemical systems in which a linear density gradient had been established employed the electrode separation  $h$  as the characteristic dimension for use in Eq. (1).

That treatment leads to a theoretical stability criterion  $Ra = 1707$ . Experimental studies by Baranowski and Kawczynski (51) point to  $Ra = 1130 \pm 210$ , which falls within the limits of the present study. However, this agreement could be regarded as fortuitous, since Baranowski and Kawczynski (a) employed the electrode separation as a characteristic dimension and (b) performed experiments in the absence of forced flow.

#### CONCLUSION

We have shown that the critical Rayleigh Number is a useful criterion to predict the occurrence of natural convection in the presence of forced convection. The numerical value of critical Rayleigh Number depends on the choice of characteristic dimension employed in Eq. (1). The present value of 1270 has been obtained with the 90% boundary layer thickness as the characteristic length. If the 99% boundary layer edge (filled circle, Fig. 7) was chosen instead, the critical Rayleigh Number would be  $Ra = 3230$ ; the Nernst boundary layer thickness would lead to  $Ra = 735$ .

TABLE 1. Onset of Natural Convection

Re	$i$ (mA/cm <sup>2</sup> )	$z_c$ (cm)	Uncertainty $\pm$ (cm)	Ra	Uncertainty $\pm$
500	2.0	8.0	1.0	1100	190
500	3.0	6.0	1.0	1120	250
500	3.8	5.0	1.0	1110	310
500	6.1	4.0	1.0	1310	450
500	10.0	3.0	1.0	1450	680
1000	3.0	12.0	1.0	1120	125
1000	4.0	14.0	4.0	1820	660
1000	5.8	8.5	1.0	1360	215
1000	10.0	5.0	1.0	1140	310
1500	3.0	20.0	5.0	1290	440
1500	4.0	14.0	4.0	1070	420
1500	10.0	8.5	1.0	1320	210

ACKNOWLEDGEMENT

This work was supported by the Director, Office of Energy Research, Office of Basic Energy Sciences, Materials Sciences Division of the U. S. Department of Energy under contract #W-7405-ENG-48.

This paper contains material that was originally presented at the 151st meeting of the Electrochemical Society, Philadelphia, Pennsylvania, May 1977, Abstract No. 304.

LIST OF SYMBOLS

C	CuSO <sub>4</sub> concentration (mole/liter)
C <sub>s</sub>	CuSO <sub>4</sub> interfacial concentration (mole/liter)
C <sub>∞</sub>	CuSO <sub>4</sub> bulk solution concentration (mole/liter)
d	glass sidewall thickness (cm)
d <sub>e</sub>	hydraulic diameter of flow channel = 1.44 cm
D	CuSO <sub>4</sub> electrolyte diffusion coefficient (cm <sup>2</sup> /s)
g	gravitational acceleration (cm/s <sup>2</sup> )
Gr	Grashof Number, $g \delta^3 \Delta\rho/\rho\nu^2$
h	electrode separation (cm)
i	current density (mA/cm <sup>2</sup> )
L	electrode length (cm)
n	electrolyte refractive index
Ra	Rayleigh Number, $Gr \cdot Sc$
Re	Reynolds Number, $d_e v_{avg}/\nu$
Sc	Schmidt Number, $\nu/D$
v <sub>avg</sub>	average electrolyte velocity (cm/s)
w	channel width (cm)
x	coordinate parallel to light propagation direction (Fig. 1) (cm)
y	coordinate normal to electrode surface (cm)
Y	$y/\delta$
z	coordinate parallel to electrolyte flow, Fig. 1 (cm)
z <sub>c</sub>	location of transition between forced convection and combined forced/natural convection control (cm)

$\alpha$	electrolyte densification coefficient ( $\text{gm/M-cm}^3$ )
$\delta$	mass transfer boundary layer thickness (cm)
$\delta_c$	characteristic boundary layer thickness (cm)
$\delta_N$	Nernst boundary layer thickness (cm)
$\Delta C$	$C_\infty - C_s$ (mole/liter)
$\Delta \rho$	$\rho_\infty - \rho_s$ ( $\text{gm/cm}^3$ )
$\theta$	dimensionless concentration $(C - C_s)/(C_\infty - C_s)$
$\mu$	electrolyte viscosity ( $\text{gm/cm-s}$ )
$\nu$	electrolyte kinematic viscosity ( $\text{cm}^2/\text{s}$ )
$\rho$	electrolyte density ( $\text{gm/cm}^3$ )
$\rho_s$	electrolyte density at electrode/electrolyte interface ( $\text{gm/cm}^3$ )
$\rho_\infty$	density of bulk electrolyte ( $\text{gm/cm}^3$ )

REFERENCES

1. V. G. Levich, *Acta Physicochim. URSS*, 19, 117 (1944).
2. J. N. Agar, *Disc. Faraday Soc.*, 1,31 (1947).
3. C. Wagner, *J. Electrochem. Soc.*, 95, 161 (1949).
4. N. Ibl and R. H. Muller, *ibid.*, 105, 346 (1958).
5. J. R. Selman and J. S. Newman, *ibid.*, 118, 1070 (1971).
6. Y. Awakura, Y. Takenaka and Y. Kondo, *Electrochim. Acta*, 21, 789 (1976).
7. N. Ibl, Y. Barrada and G. Trumpler, *Helv. Chim Acta*, 37, 583 (1954).
8. T. Yannakopoulos and A. Brenner, *J. Electrochem. Soc.*, 105, 521 (1958).
9. Y. Awakura and Y. Kondo, *ibid.*, 123,1184 (1976).
10. Y. Awakura, M. Okada and Y. Kondo, *ibid*, 124, 1050 (1977).
11. C. R. Wilke, M. Eisenberg and C. W. Tobias, *ibid.*, 100,513 (1953).
12. N. Ibl, W. Ruegg and G. Trumpler, *Helv. Chim. Acta*, 36, 1624 (1953).
13. K. Asada, F. Hine, S. Yoshizawa and S. Okada, *J. Electrochem. Soc.*, 107, 242 (1960).
14. D. J. Pickett and B. R. Stanmore, *J. Appl. Electrochem.*, 2,151 (1972).
15. S. Mohanta and T. Z. Fahidy, *Can. J. Chem. Eng.*, 50, 248 (1972).
16. E. Schalch and N. Ibl, *Electrochim. Acta*, 20, 435 (1975).
17. W. H. Safranek and C. H. Layer, *Trans. Inst. Metal Finish.*, 53, 121 (1975).
18. W. R. Wolfe, H. Chessin, E. Yeager and F. Hovorka, *J. Electrochem. Soc.*, 101, 590 (1954).
19. S. Eisner, *Plating*, 58, 995 (1971).
20. C. W. Tobias and R. G. Hickman, *Z. Physik. Chem.*, 229, 145 (1965).
21. R. H. Muller in Advances in Electrochemistry and Electrochemical Engineering, R. H. Muller, ed., Wiley-Interscience, N.Y., 1973, Vol. 9, p.p. 326-353.
22. W. Hauf and U. Grigull in Advances in Heat Transfer, J. P. Hartnett and T. F. Irvine, eds., Academic Press, N.Y. 1970, Vol. 6, p.p.133-366.

23. F. R. McLarnon, Ph.D. Thesis, LBL-3500, Univ. of California, Berkeley, 1975.
24. C. S. Lin, R. W. Moulton and G. L. Putnam, Ind. Eng. Chem., 45, 640 (1953).
25. N. Ibl and R. H. Muller, Z. Elektrochem., 59, 671 (1955).
26. R. N. O'Brien, W. F. Yakymyshyn and J. Leja, J. Electrochem. Soc., 110, 820 (1963).
27. R. N. O'Brien, *ibid.*, 111, 1300 (1964).
28. R. N. O'Brien, *ibid.*, 113, 389 (1966).
29. L. Hsueh and J. S. Newman, Electrochim. Acta, 16, 479 (1971).
30. A. Tvarusko and L. S. Watkins, J. Electrochem. Soc., 118, 248 (1971).
31. F. R. McLarnon, R. H. Muller and C. W. Tobias, Electrochim Acta, 21, 101 (1976).
32. F. R. McLarnon, R. H. Muller and C. W. Tobias, Ind. Eng. Chem. Fund. 18, 97 (1979).
33. M. Clifton and V. Sanchez, Electrochim. Acta 24, 445 (1979).
34. E. V. Heydebrand, Ann. der Physik, (5), 37, 589 (1940).
35. U. Grigull, Int. J. Heat Mass Transfer, 6, 669 (1963).
36. G. D. Kahl and D. C. Mylin, J. Opt. Soc. Am., 55, 364 (1965).
37. W. L. Howes and D. R. Buchele, *ibid.*, 56, 1517 (1966).
38. K. W. Beach, R. H. Muller and C. W. Tobias, *ibid.*, 63, 559 (1973).
39. F. R. McLarnon, R. H. Muller and C. W. Tobias, J. Electrochem. Soc. 122, 59, (1975).
40. F. R. McLarnon, R. H. Muller and C. W. Tobias, J. Opt. Soc. Am., 65, 1011 (1975).
41. E. E. Anderson, W. H. Stevenson and R. Viskanta, Appl. Optics, 14, 185 (1975).
42. A. M. Hunter and P. W. Schreiber, *ibid.*, p. 634.
43. C. M. Vest, *ibid.*, p. 1601.

44. K. W. Beach, Ph.D. Thesis, UCRL-20324, University of California, Berkeley, 1971.
45. K. W. Beach, R. H. Muller and C. W. Tobias, Rev. Sci. Inst. 40, 1248 (1969).
46. F. R. McLarnon, R. H. Muller and C. W. Tobias, Appl. Optics 14, 2468 (1975).
47. R. H. Norris and D.D. Streid, Trans. ASME 62, 525 (1940).
48. T. W. Chapman and J. S. Newman, "A Compilation of Selected Thermodynamic and Transport Properties of Binary Electrolytes in Aqueous Solutions", Lawrence Berkeley Laboratory. Report No. UCRL-17767, May 1968, p.p.37-39.
49. J. S. Newman, "Electrochemical Systems," p. 395, Prentice-Hall, Englewood Cliffs, 1973.
50. B. Baranowski and A. L. Kawczynski, Roczn. Chem. 44, 2447 (1970).
51. B. Baranowski and A. L. Kawczynski, Electrochim. Acta. 17, 695 (1972).

FIGURE CAPTIONS

Figure 1: Semi-scale drawing of the flow channel: channel width  $w = 10.0$  mm, channel height  $h = 25.4$  mm, and electrode length  $L = 100.0$  cm.

Figure 2: Interferometer and electrochemical cell cross section: —, light path; ---, off-axis rays demonstrating point-to-point relationship between plane of focus and film plane; A, copper anode; C, copper cathode; E, 0.1 M  $\text{CuSO}_4$  electrolyte; F, film plane; G, glass sidewalls; L, lens (The test lens, focal length=87 mm, is 115 mm from the center of the cell. The focal length of the reference lens is 81 mm); M, mirror; S, light source (HeNe laser); U, beam uniter; d, thickness of glass wall (12.7 mm); h, electrode separation (25.4 mm); w, electrode width (10.0 mm).

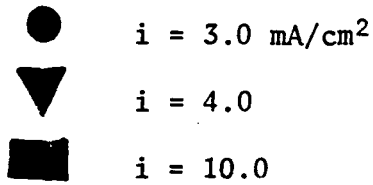
Figure 3: Experimental interferograms showing transient boundary layer growth. Ordinate: vertical distance from cathode surface (mm). The true cathode surface is identified by "0". The cathode faces down in the four interferograms in the upper half. It faces up in the lower half of this figure.

Figure 4: Variation of boundary layer thickness,  $Re = 500$ . Ordinate: Nernst boundary layer thickness (mm). Abscissa: Reduced distance from cathode leading edge. Open Symbols: Derived from experimental interferograms, cathode faces down. Filled Symbols: Derived from experimental interferograms, cathode faces up.

 	$i = 2.0 \text{ mA/cm}^2$
	$i = 3.8$
	$i = 6.1$

— Norris and Streid correlation.  
- - - - Boundary layer thinned by superimposed natural convection.

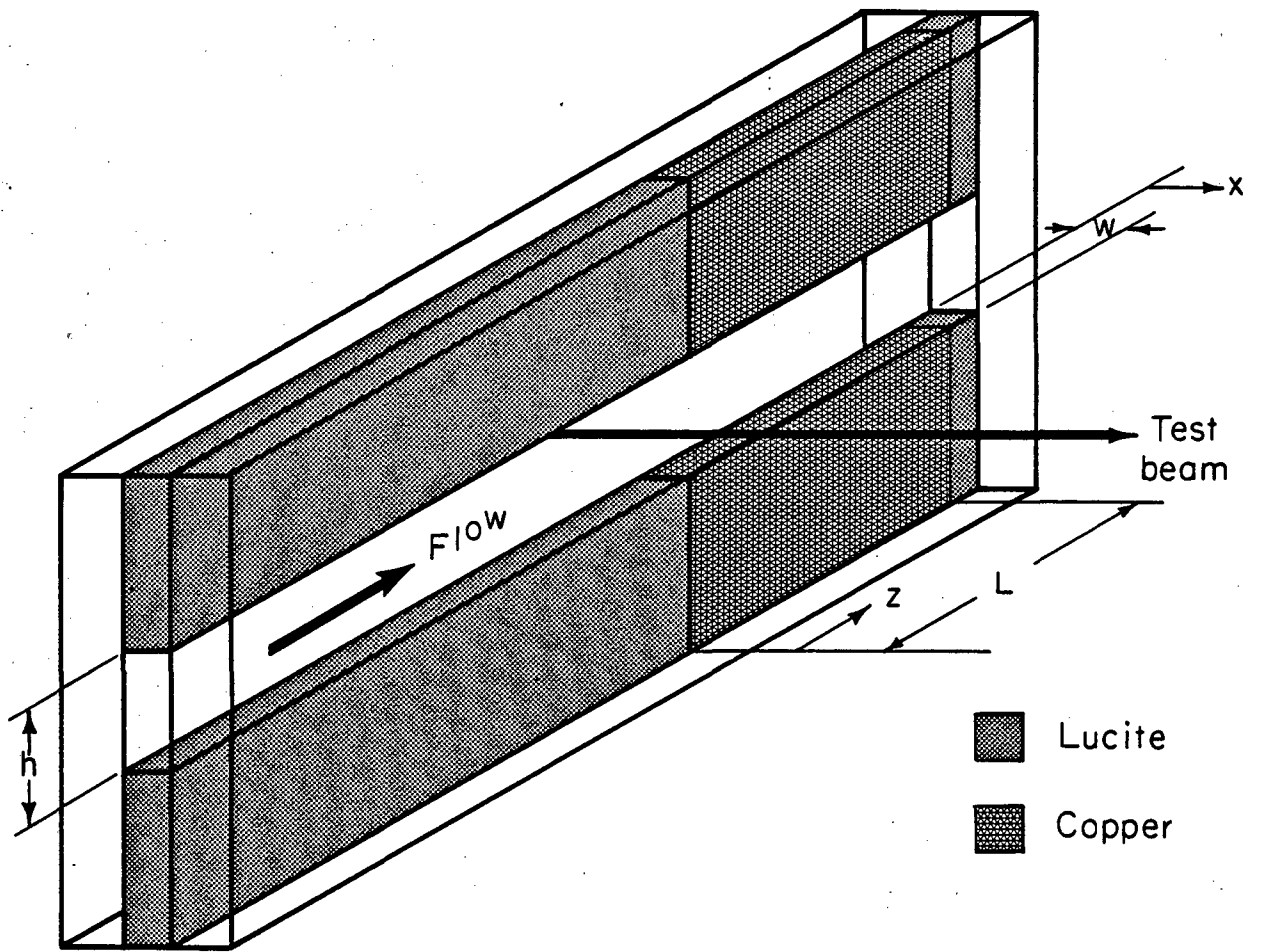
Figure 5: Variation of boundary layer thickness,  $Re = 1500$ .



Other designations as in Fig. 4.

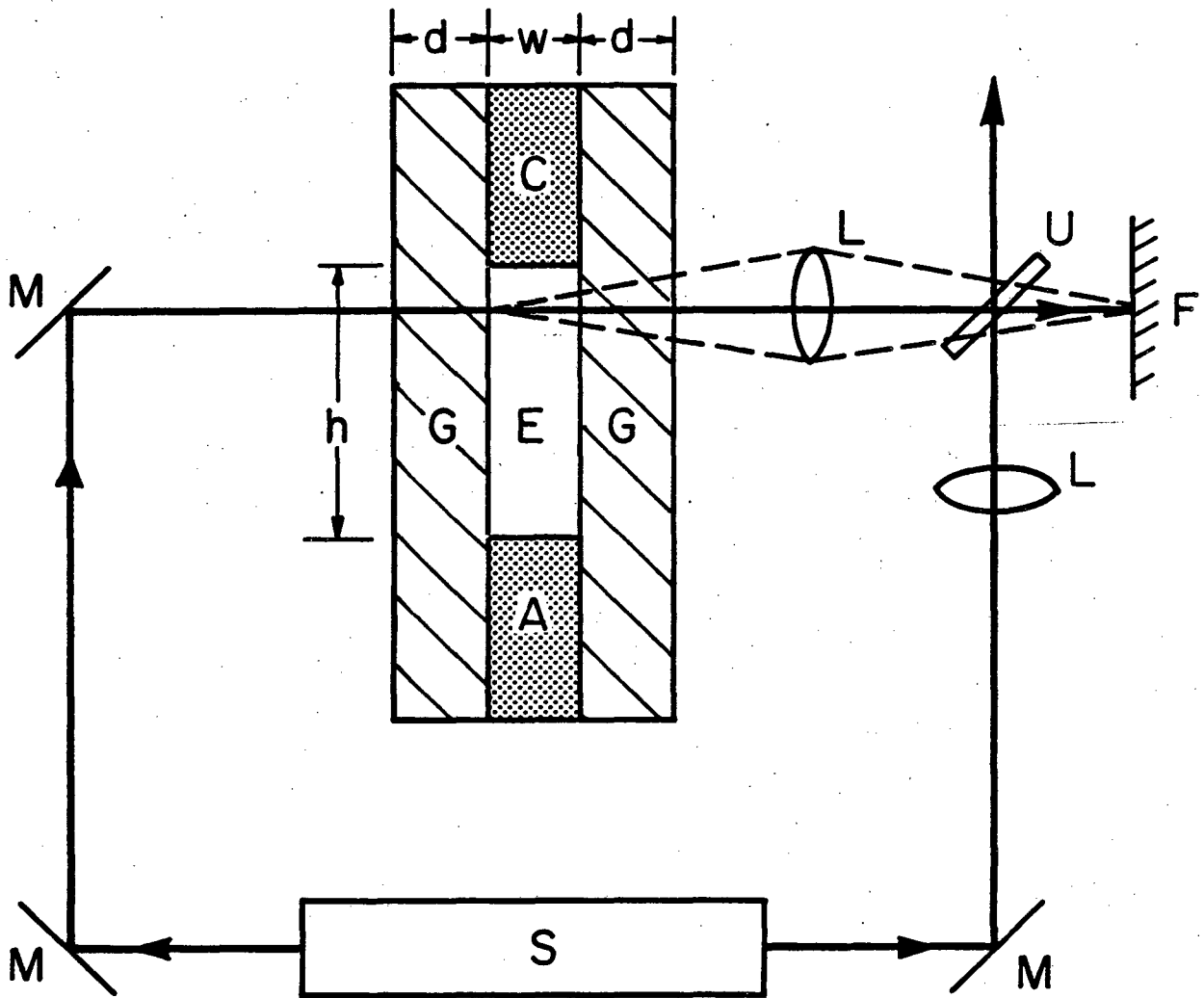
Figure 6: Smoothed limiting current densities obtained by Tobias and Hickman (20).  
Ordinate: limiting current density.  
Abscissa: distance downstream from cathode leading edge.

Figure 7: Pohlhausen -type concentration profile  
Ordinate: Reduced distance,  $y/\delta$   
Abscissa: Dimensionless concentration,  $(C-C_S)/(C_\infty-C_S)$   
———— Pohlhausen profile Eq. (3).  
- - - - "Equivalent" boundary layer for the 90% boundary layer edge.  
- - - - Nernst boundary layer  
○ 90% boundary layer edge  
● 99% boundary layer edge



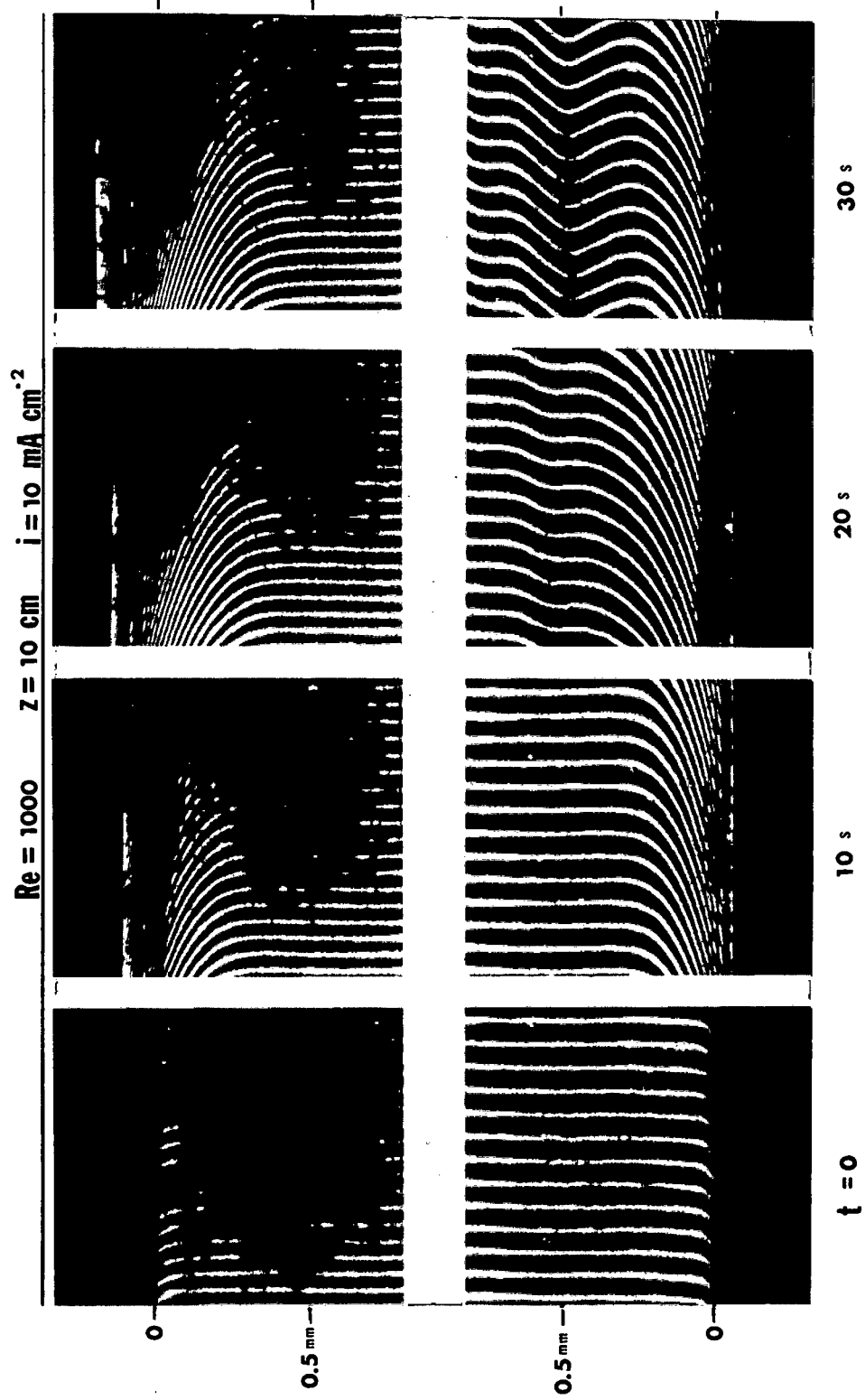
XBL 7410 - 4480

Figure 1



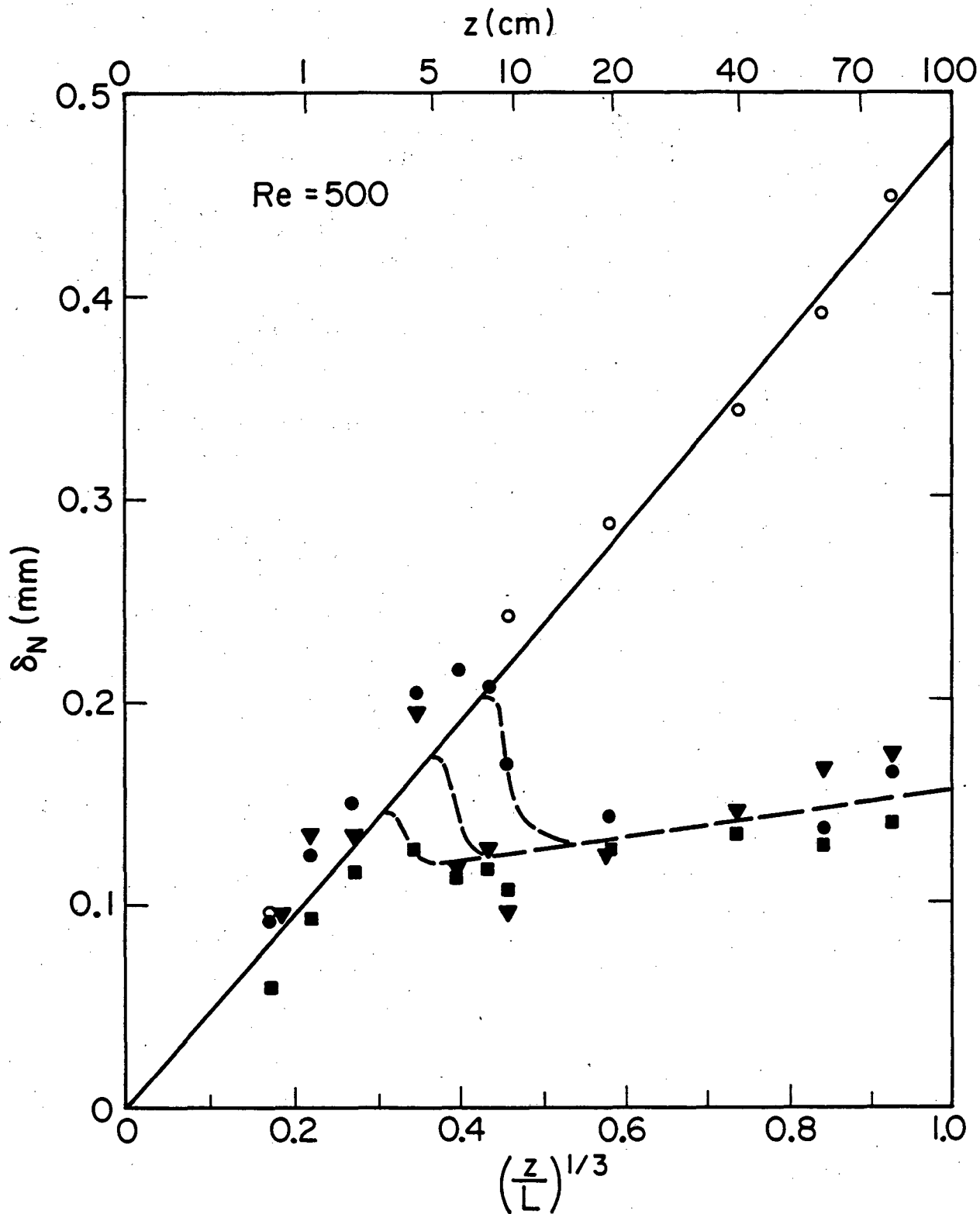
XBL749-4165

Figure 2



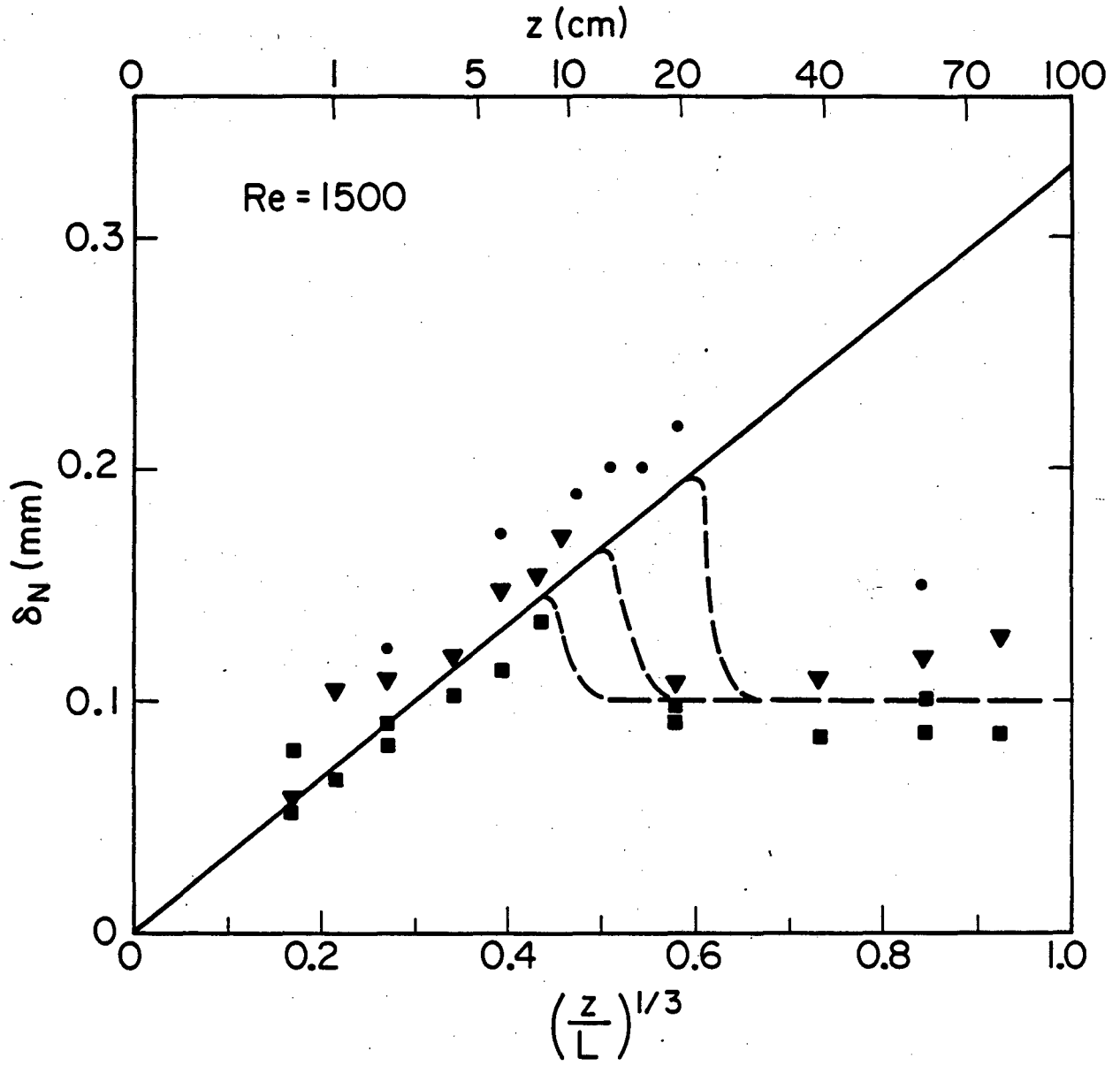
XBB 748-5799

Figure 3



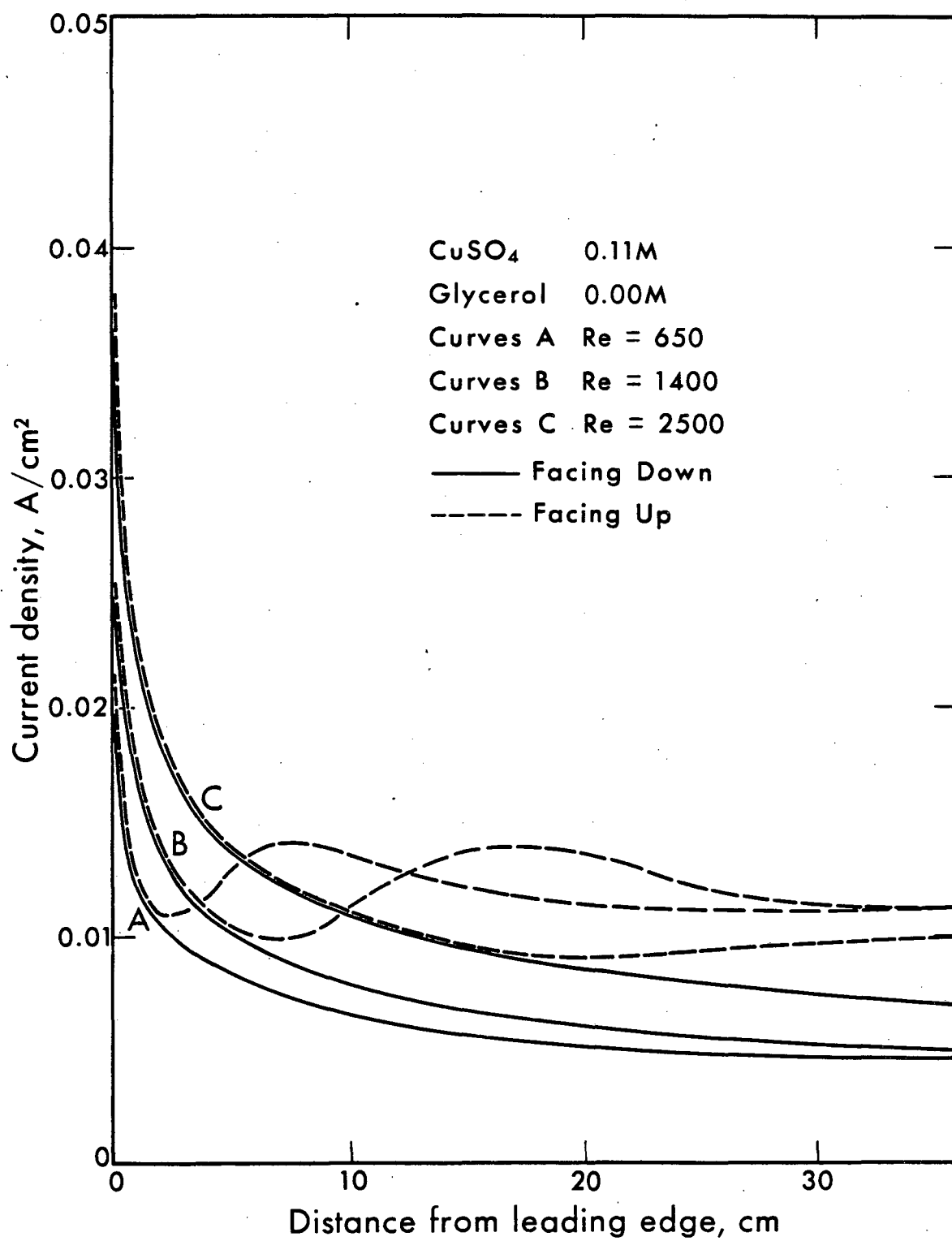
XBL7411-8224

Figure 4



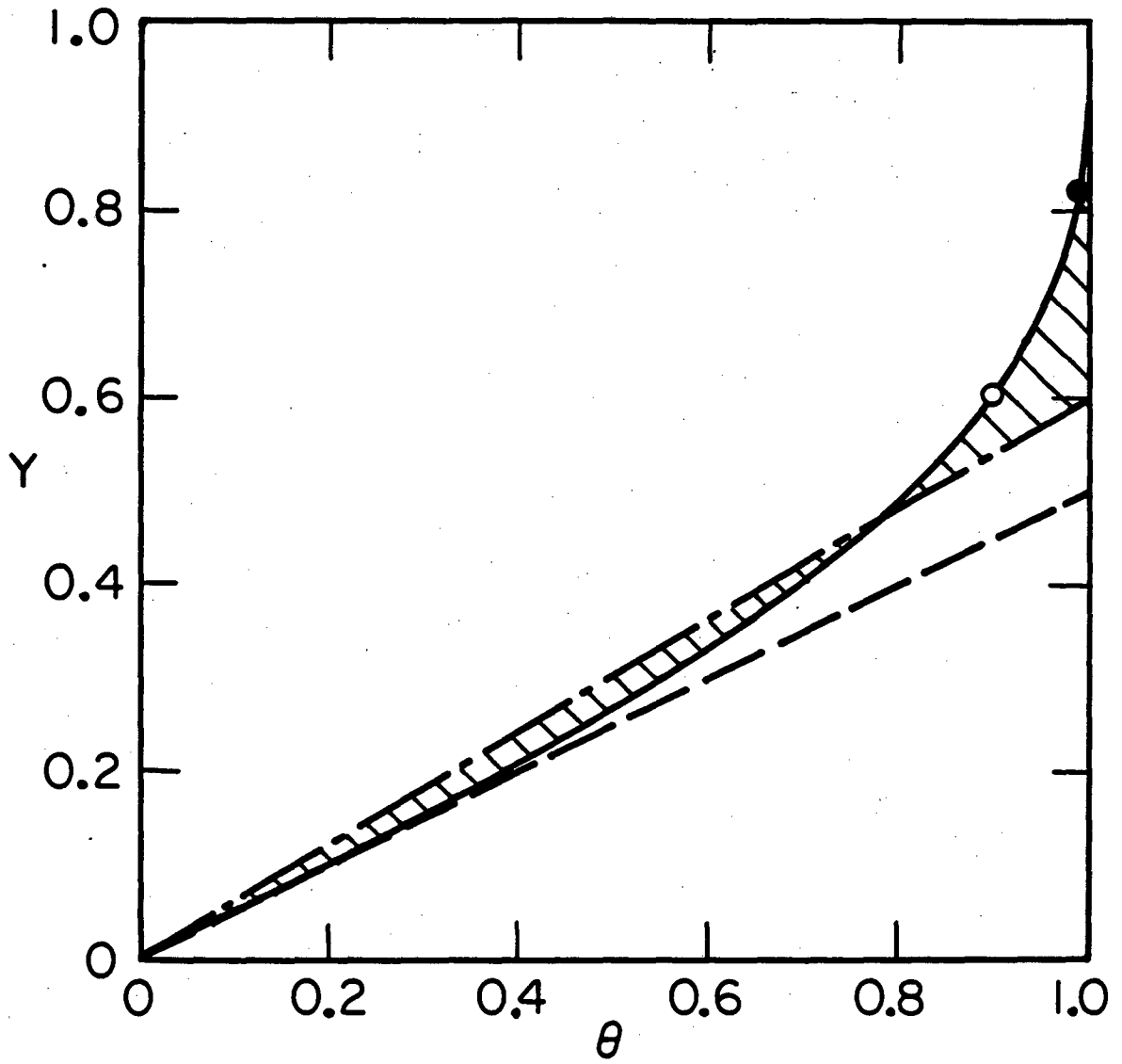
XBL7411-8223

Figure 5



XBL 7411-8618

Figure 6



XBL7411-4577

Figure 7

This report was done with support from the Department of Energy. Any conclusions or opinions expressed in this report represent solely those of the author(s) and not necessarily those of The Regents of the University of California, the Lawrence Berkeley Laboratory or the Department of Energy.

Reference to a company or product name does not imply approval or recommendation of the product by the University of California or the U.S. Department of Energy to the exclusion of others that may be suitable.

TECHNICAL INFORMATION DEPARTMENT  
LAWRENCE BERKELEY LABORATORY  
UNIVERSITY OF CALIFORNIA  
BERKELEY, CALIFORNIA 94720